Purdue University

Purdue e-Pubs

International Refrigeration and Air Conditioning Conference

School of Mechanical Engineering

2022

Dynamic Modeling of Air Source Heat Pumps under Reverse-cycle Defrosting

Jiacheng Ma

Donghun Kim

James E. Braun

Follow this and additional works at: https://docs.lib.purdue.edu/iracc

Ma, Jiacheng; Kim, Donghun; and Braun, James E., "Dynamic Modeling of Air Source Heat Pumps under Reverse-cycle Defrosting" (2022). *International Refrigeration and Air Conditioning Conference*. Paper 2325.
https://docs.lib.purdue.edu/iracc/2325

This document has been made available through Purdue e-Pubs, a service of the Purdue University Libraries. Please contact epubs@purdue.edu for additional information.
Complete proceedings may be acquired in print and on CD-ROM directly from the Ray W. Herrick Laboratories at https://engineering.purdue.edu/Herrick/Events/orderlit.html

Dynamic Modeling of Air Source Heat Pumps under Reverse-cycle Defrosting

Jiacheng Ma[1*], Donghun Kim[2], James E. Braun[1],

[1] Ray W. Herrick Laboratories, School of Mechanical Engineering, Purdue University,
West Lafayette, IN, U.S.
ma516@purdue.edu, jbraun@purdue.edu

[2] Building Technology & Urban Systems Division, Lawrence Berkeley National Laboratory,
Berkeley, CA, U.S.
donghunkim@lbl.gov

* Corresponding Author

ABSTRACT

One of the biggest challenges associated with air source heat pump units is the performance degradation and inefficiency due to frost accumulation on the outdoor coil surface. The continued buildup of frost eventually necessitates a defrosting mode to remove the accumulated frost and return the system to its normal operating characteristics. Dynamic modeling of a defrost cycle is extremely useful in development and evaluation of improved defrost control designs. Most of the previous modeling studies solely focused on the heat and mass transfer characteristics on the air side neglecting the corresponding dynamics of the reverse refrigerant flow and have not considered complete transient systems simulations with experimental validations. In this work, a comprehensive dynamic modeling framework is presented to investigate the transient characteristics of a residential heat pump under reverse-cycle defrosting operations. A smooth transition scheme is applied to the frost melting model, which is typically described by multi-stage sub-models, to improve model robustness. A transient simulation is conducted, and results are compared against measurement data for a residential heat pump unit. The model presented can be used to conduct performance evaluations of the defrosting cycle, as well as energy assessments for comparisons of different defrost strategies.

1. INTRODUCTION

Frost accumulation on evaporator coil surfaces can significantly degrade the performance of air-source heat pump (ASHP) systems in winter operations. The continued buildup of frost eventually necessitates a defrosting mode to remove the accumulated frost and return the system to its normal operating characteristics. Among various approaches currently employed on ASHP systems, reverse-cycle defrosting (RCD) that applies heat to the outdoor coil by reversing the thermodynamic cycle, is one of the predominant means because of its easy implementation without additional heat sources. Dynamic modeling of ASHP under defrosting operations is extremely useful in development and evaluation of improved defrost control algorithms. Despite the straightforward concept of RCD, significant computational complexities are involved due to reverse refrigerant flow and coupled dynamics of frost and the refrigerant cycle. A literature screening indicates that there is a very limited number of system-level modeling efforts. Many studies solely focused on performance of heat exchangers during RCD, e.g., (Qu et al., 2012; Dopazo et al., 2010). Within the context of complete cycle modeling considering the dynamics on both the refrigerant side and air side, Steiner and Rieberer (2013) simulated the defrosting process of a CO2 heat pump system used for an electric vehicle by integrating a lumped frost melting model into the heat exchanger model. Predictions of the refrigerant dynamics and the compressor power showed reasonable agreements with the measurements. Then the model was used to conduct a parametric analysis on different expansion valve openings during defrosting. It was found that an optimal valve opening existed regarding defrost time and efficiency. However, only the system operation after the refrigerant pressure levels were equalized and the compressor was turned on again in defrost cycle, was simulated omitting the reverse flow transients. Han et al. (2022) carried out a simulation study of a residential heat pump system during defrosting cycles. A multi-stage frost melting model was coupled to a finite volume heat exchanger model. Results were compared with experimental data and yielded good agreement. Similar to Steiner and Rieberer (2013), both studies concentrated on system dynamics during a short time period of the defrosting cycle, and excluded the refrigerant pressure equalization stage triggering flow reversal. In a subsequent simulation study, Qiao et al. (2018) incorporated a multi-stage frost melting model in the

evaporator model. With a reversing valve model, the system model was able to capture transients when the refrigerant flow was reversed during initiation and termination of RCD. No experimental validation was provided.

The objective of this paper is to develop and experimentally validate transient models for ASHP under RCD operations, that is directly applicable to development and evaluation of controls. This paper presents component models to complete a heat pump cycle model that can capture the flow reversal and defrost dynamics. To improve model robustness, a general switching scheme for multi-stage frost melting models is proposed that can systematically cover all possible switches and ensures smooth transitions. The heat pump cycle model is simulated to predict dynamics switching from heating mode to RCD and then back to heating mode. Simulation results are compared with measurements collected from a residential heat pump unit. The reminder of this paper is organized as follows. Section 2 presents a frost melting model and component models to complete an ASHP cycle model for RCD simulations. Section 3 describes the RCD dynamics and model validations. Conclusions of the present work are summarized in Section 4.

2. MATHEMATICAL MODEL

Building upon development of an ASHP cycle model presented in Ma et al. (2022), a frost melting model is incorporated into the heat exchanger model to capture system behaviors during RCD. Furthermore, a reversing valve model is integrated into the cycle model, which is essential to switch between heating and defrosting modes.

2.1 Frost Melting

One-dimensional multi-stage frost melting models have been introduced to approximate the rather stochastic defrost process in existing studies, that the defrost process progresses through several predicable stages (Qiao et al., 2018; Dopazo et al., 2010; Qu et al., 2012; Mohs, 2013). As a result, the model is composed of case-by-case mathematical descriptions, and switches between different stages. Each stage is described by a set of governing equations according to the current temperature profile and phase presence. The present work applies a five-stage defrost model subdividing the overall process into preheating, melting start, melting, vaporizing, and dry heating (Qiao et al., 2018). The model is basically established by a lumped-capacitance analysis along with energy and mass conservation at interfaces. The governing equations of the preheating stage are:

$$\rho_f c_{p,f} \delta_f \frac{dT_f}{dt} = k_f \frac{T_w + T_{fs} - 2T_f}{\delta_f/2} \tag{1}$$

$$k_f \frac{T_f - T_{fs}}{\delta_f/2} = q_a'' \tag{2}$$

where T_w is the metal wall temperature, T_f is the lumped frost layer temperature, δ_f is the frost layer thickness, T_{fs} is the temperature of the frost-air interface, q_a'' is the heat flux transferred to the surrounding air. At this stage the wall surface temperature is still below the freezing point of water (273.15 K in the following equations), which indicates that no phase change occurs. As the frost starts to thaw, a water film appears between the wall and the frost layer. It is assumed that temperature of the water-frost interface remains at 273.15 K. This stage terminates until the maximum amount of water that can be retained on the coil surface is reached. The maximum water film thickness is set to $\delta_{water,max}$ = 0.05 mm (Qiao et al., 2018). The governing equations of the melting start stage are (2), (3)-(6)

$$\rho_{water} c_{p,water} \delta_{water} \frac{dT_{water}}{dt} = k_{water} \frac{T_w + 273.15 - 2T_{water}}{\delta_{water}/2} \tag{3}$$

$$\rho_f c_{p,f} \delta_f \frac{dT_f}{dt} = k_f \frac{273.15 + T_{fs} - 2T_f}{\delta_f/2} \tag{4}$$

$$-\rho_f \Delta h_{sf} \frac{d\delta_f}{dt} = k_{water} \frac{T_{water} - 273.15}{\delta_{water}/2} - k_f \frac{273.15 - T_f}{\delta_f/2} \tag{5}$$

$$\rho_{water} \frac{d\delta_{water}}{dt} = -\rho_f \frac{d\delta_f}{dt}, \tag{6}$$

where T_{water} is the water film temperature, δ_{water} is the water film thickness, the latent heat of fusion Δh_{sf} is 334 kJ/kg. The frost continues to thaw during the melting stage. The melted water is assumed to be drained immediately, resulting in the development of an air gap between the water film and the frost. The temperature of the air-frost interface remains

at 273.15 K. The governing equations of this stage are (2), (4), (7)-(11)

$$\rho_{water} c_{p,water} \delta_{water} \frac{dT_{water}}{dt} = k_{water} \frac{T_w - T_{water}}{\delta_{water}/2} - \frac{T_{water} - T_a}{\frac{\delta_{water}}{2k_{water}} + \frac{\delta_a}{2k_a}} \tag{7}$$

$$\rho_a c_{p,a} \delta_a \frac{dT_a}{dt} = \frac{T_{water} - T_a}{\frac{\delta_{water}}{2k_{water}} + \frac{\delta_a}{2k_a}} - k_a \frac{T_a - 273.15}{\delta_a/2} \tag{8}$$

$$-\rho_f \Delta h_{sf} \frac{d\delta_f}{dt} = k_a \frac{T_a - 273.15}{\delta_a/2} - k_f \frac{273.15 - T_f}{\delta_f/2} \tag{9}$$

$$\frac{d\delta_a}{dt} = -\frac{d\delta_f}{dt} \tag{10}$$

$$\frac{d\delta_{water}}{dt} = 0 \tag{11}$$

where T_a is the air gap temperature and δ_a is the air gap thickness. The governing equations of the vaporizing stage are

$$\rho_{water} c_{p,water} \delta_{water} \frac{dT_{water}}{dt} = k_{water} \frac{T_w + T_{water,s} - 2T_{water}}{\delta_{water}/2} \tag{12}$$

$$\rho_{water} \frac{d\delta_{water}}{dt} = c_v (\rho_{amb} - \rho_{water,s}) \tag{13}$$

$$k_{water} \frac{T_{water} - T_{water,s}}{\delta_{water}/2} = q_a'' \tag{14}$$

$$\frac{\delta_f}{dt} = 0 \tag{15}$$

$$\frac{\delta_a}{dt} = 0 \tag{16}$$

where ρ_{amb} and $\rho_{water,s}$ are water vapor densities evaluated at the ambient temperature and the water layer surface temperature $T_{water,s}$, respectively. c_v is the vaporization coefficient. During the dry heating stage, heat is directly dissipated from the metal wall to the ambient air. Variables of thicknesses and temperatures in the frost melting model are inactive. The overall melting process is illustrated in Figure 1.

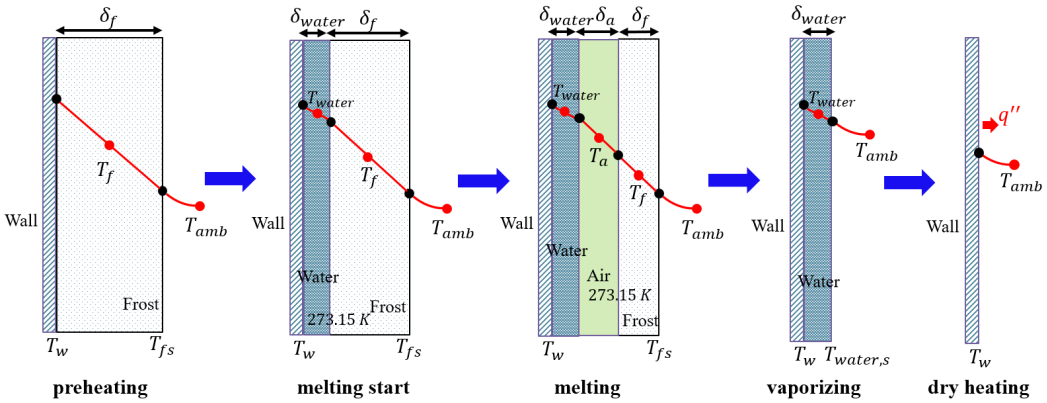

Figure 1: Five-stage frost melting process.

For the sake of model consistency, prior to the appearance of the water film and air gap, dynamics of the corresponding thicknesses and temperatures are inactive. While the thickness dynamics can simply be set to zero, a pseudo governing equation can be applied to the temperature dynamics. For example, the temperature of the air gap during the melting start stage is evaluated by

$$\frac{dT_a}{dt} = \frac{1}{\tau}(T_{water} - T_a) \tag{17}$$

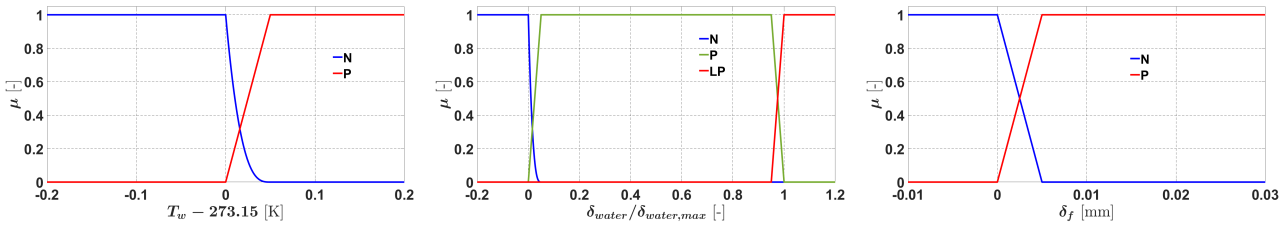

Figure 2: Fuzzy numbers and membership functions for linguistic variables: (a) $T_w - 273.15$, (b) $\delta_{water}/\delta_{water,max}$, (c) δ_f.

where τ is a time constant. Its function is to provide a reasonable initial condition by tracking the water film temperature until the air gap temperature becomes active. In addition, the frost density is assumed to remain constant throughout the melting process, however, it is desired to reset the density to an initial value (e.g., $\rho_{f,\text{init}} = 25\,\text{kg/m}^3$) before frost growth in heating cycles if all the frost is melted during RCD. This can be resolved by adding dynamics of the frost density to the model. A filter is used to achieve this goal

$$\frac{d\rho_f}{dt} = \frac{1}{\tau}(\rho_{f,\text{init}} - \rho_f). \tag{18}$$

(18) is added to the governing equations of the vaporizing stage and the dry heating stage, while the frost density dynamics of other stages are simply set to zero. Consequently, each stage can be represented by the following state vector:

$$x = \begin{bmatrix} T_f & \delta_f & T_{water} & \delta_{water} & T_a & \delta_a & \rho_f \end{bmatrix}^T. \tag{19}$$

Transitions between different stages can be achieved by a set of IF-THEN rules. Qiao et al. (2018) applied an interpolation scheme that smoothed the transition by computing a weighted average of the dynamics and thus avoided discontinuities. However, any possible transition between two stages needs to be treated in this way, which requires a complicated set of rules. It is important to note that Figure 1 shows the ideal model behavior, however, the actual simulation may not proceed in this order due to the rapidly evolving refrigerant dynamics during flow reversal. Therefore, a general and reliable switching algorithm is necessary to avoid the discontinuities and improve model robustness. In the present work, the Fuzzy Modeling approach is adopted (Kim et al., 2021). Recall that based on the assumptions applied to derive the frost melting model, transitions between different stages involve the metal wall temperature T_w and state variables δ_f and δ_{water}. Define three linguistic variables $T_w - 273.15$, $\delta_{water}/\delta_{water,max}$ and δ_f. Fuzzy numbers and their associated membership functions are constructed for each variable as depicted in Figure 2. Denote the governing equations of each stage as $f_i(x)$ ($i = \{1,2,3,4,5\}$). The following linguistic descriptions in terms of IF-THEN rules can be applied to determine the system dynamics:

Rule 1: IF $T_w - 273.15$ is N THEN $\dot{x} = f_1(x)$,

Rule 2: IF ($T_w - 273.15$ is P) and ($\delta_{water}/\delta_{water,max}$ is N or $\delta_{water}/\delta_{water,max}$ is P) and (δ_f is P) THEN $\dot{x} = f_2(x)$,

Rule 3: IF ($T_w - 273.15$ is P) and ($\delta_{water}/\delta_{water,max}$ is LP) and (δ_f is P) THEN $\dot{x} = f_3(x)$,

Rule 4: IF ($T_w - 273.15$ is P) and ($\delta_{water}/\delta_{water,max}$ is LP or $\delta_{water}/\delta_{water,max}$ is P) and (δ_f is N) THEN $\dot{x} = f_4(x)$,

Rule 5: IF ($T_w - 273.15$ is P) and ($\delta_{water}/\delta_{water,max}$ is N) and (δ_f is N) THEN $\dot{x} = f_5(x)$.

These given IF-THEN rules are subsequently converted into numerical outputs of the system dynamics, known as the *defuzzification* process. The center average defuzzifier (product inference rule) is used (Zak, 2003), as described in (20)

$$\dot{x} = \frac{\sum_{i=1}^{5} \omega_i f_i(x)}{\sum_{i=1}^{5} \omega_i} \tag{20}$$

where ω_i can be obtained by

$$\omega_1 = \mu_N(T_w - 273.15) \tag{21}$$

$$\omega_2 = \mu_P(T_w - 273.15) \times \left(\mu_N(\delta_{water}/\delta_{water,max}) + \mu_P(\delta_{water}/\delta_{water,max})\right) \times \mu_P(\delta_f) \tag{22}$$

$$\omega_3 = \mu_P(T_w - 273.15) \times \mu_{LP}(\delta_{water}/\delta_{water,max}) \times \mu_P(\delta_f) \tag{23}$$

$$\omega_4 = \mu_P(T_w - 273.15) \times \left(\mu_{LP}(\delta_{water}/\delta_{water,max}) + \mu_P(\delta_{water}/\delta_{water,max})\right) \times \mu_N(\delta_f) \tag{24}$$

$$\omega_5 = \mu_P(T_w - 273.15) \times \mu_N(\delta_{water}/\delta_{water,max}) \times \mu_N(\delta_f). \tag{25}$$

It can be observed that IF-THEN rules are completely eliminated throughout the defuzzification process, and the final model is in a weighted combination form of dynamics from all the stages. Interface variables of the frost melting model with the metal wall and air flow models are determined in a weighted way as well. The temperature of the surface exposed to air is calculated considering the medium presence of each stage:

$$T_{as} = \left(\sum_{i=1}^{3} \omega_i\right) T_{fs} + \omega_4 T_{water,s} + \omega_5 T_w \tag{26}$$

where T_{as} is the surface temperature used to determine the air side heat and mass transfer. Similarly, the heat flux transfer with the metal wall is calculated by

$$q''_w = \omega_1 k_f \frac{T_w - T_f}{\delta_f/2} + \left(\sum_{i=2}^{4} \omega_i\right) k_{water} \frac{T_w - T_{water}}{\delta_{water}/2} + \omega_5 q''_{\text{dry}}, \tag{27}$$

where q''_{dry} is the heat flux under the dry heating condition, which is directed calculated by convective heat transfer.

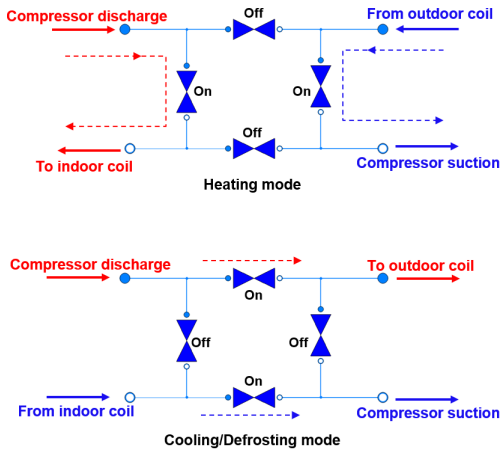

Figure 3: Model representation of a reversing valve.

2.2 Reversing Valve

It is challenging to model the exact physical process of a reversing valve, since it mainly involves mechanical movements. In the current work, two pairs of check valves are used to represent the reversing valve model (Qiao et al., 2015). As shown in Figure 3, each port of the reversing valve has a pair of check valves to control the flow direction.

One is kept fully opened, while the other is closed. When the on-off statuses of them are switched, the refrigerant flow direction is reversed. A check valve is modeled as

$$\dot{m} = \begin{cases} \varphi A_v \sqrt{2\rho_{\text{in}}(p_{\text{in}} - p_{\text{out}})} & p_{\text{in}} > p_{\text{out}} \\ 0 & p_{\text{in}} \leq p_{\text{out}} \end{cases} \tag{28}$$

where A_v is the fully opened area, φ is valve opening degree normalized between 0 and 1. When reverse flow needs to be triggered, opening and closing a check valve is achieved by changing the valve opening. However, this process is not instantaneous during mode switching. For numerical stability concerns, a first-order filter is applied to smooth the transition,

$$\frac{d\varphi}{dt} = \frac{1}{\tau}(\varphi_{SP} - \varphi) \tag{29}$$

where φ_{SP} is the opening setpoint, which is either 1 or 0 depending on the on/off status of each check valve. The heat loss from the high pressure side is primarily driven by the temperature difference between the discharge gas and the suction gas, and can be characterized by heat transfer loss/gain coefficients (Damasceno et al., 1991).

2.3 Heat Exchanger Integrated with Frost

To capture the system dynamics during mode switching operations between heating and defrosting as well as during RCD, the frost melting model is integrated into the finite-volume heat exchanger model developed in Ma et al. (2022) where a frost formation model is included. The frost formation and melting models are simultaneously running during online simulations, and the overall frost dynamics are evaluated as a weighted combination of dynamics obtained from these two models, according to the system operating mode. Since the frost density and thickness characterize its dynamics, they are selected as internal states. The overall frost dynamics of a control volume are evaluated by

$$\frac{d\rho_{f,i}}{dt} = \varphi f_{\rho,\text{form}}(\rho_{f,i}, \delta_{f,i}) + (1-\varphi) f_{\rho,\text{melt}}(\rho_{f,i}, \delta_{f,i}) \tag{30}$$

$$\frac{d\delta_{f,i}}{dt} = \varphi f_{\delta,\text{form}}(\rho_{f,i}, \delta_{f,i}) + (1-\varphi) f_{\delta,\text{melt}}(\rho_{f,i}, \delta_{f,i}) \tag{31}$$

where $f_{\rho,\text{form}}(\rho_{f,i}, \delta_{f,i})$ and $f_{\delta,\text{form}}(\rho_{f,i}, \delta_{f,i})$ are the frost formation dynamics described in Ma et al. (2022), $f_{\rho,\text{melt}}(\rho_{f,i}, \delta_{f,i})$ and $f_{\delta,\text{melt}}(\rho_{f,i}, \delta_{f,i})$ are the dynamics obtained from the frost melting model, φ is a variable that switches the frost dynamics between frost formation and melting. The reversing valve opening in (29) can be used for this purpose. The developed models are integrated into the heat pump cycle model that is implemented using the Modelica language, as shown in Figure 4.

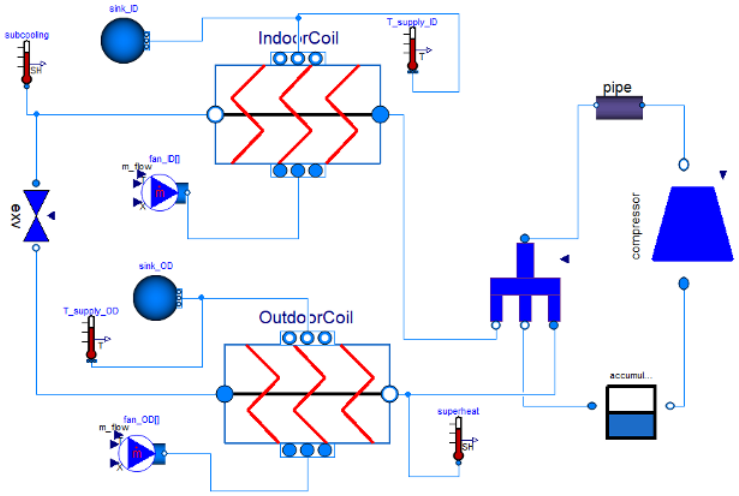

Figure 4: Heat pump cycle model implemented in Modelica.

3. VALIDATIONS

This section presents simulation results and experimental validations of the developed cycle model for capturing transient characteristics of a residential heat pump system under defrosting operations. The heat pump unit was turned on in heating mode, and operated for 30 minutes, followed by a defrost cycle lasting about 5 minutes, then normal heating operation for 120 minutes before initiating the second defrost cycle, and then another heating operation. This paper focuses on the system dynamics during the second defrost cycle and transitions between heating and defrosting operations triggering reverse refrigerant flow.

Figure 5 reports validations of the refrigerant discharge and suction pressures. The unit switches to defrost mode at 158 min after operating in heating mode for two hours with considerable frost buildup on the outdoor coil. When the system initiates RCD operation, the expansion valve is fully opened, which leads to a dramatic pressure change due to the pressure equalization across the expanion valve. Shortly the reversing valve is energized, which further brings down the discharge pressure, and slightly increases the suction pressure due to the connection to the high pressure side when the valve is switching port positions. After the flow is reversed, the discharge gas is pumped into the outdoor coil, which operates as a condenser, and the liquid refrigerant residing in the indoor coil, which operates as an evaporator, vaporizes due to the abrupt pressure drop and flows towards the vapor line. As a consequence, the discharge and suction pressures increase until termination of the defrost mode at around 170 min. Then the reversing valve is energized again to switch the flow directions, that reduces the pressure difference between the high pressure side and the low pressure side. Meanwhile, the expansion valve opening is reset to an initial position, and then adjusted following superheat control. The compressor runs at a lower speed during RCD than in heating mode. As the system switches back to heating mode, the compressor speed increases to the desired setting for heating operations, which results in the rapid rise of the discharge pressure. After that, rise of the discharge pressure slows down, which is mainly attributed to the mass flow imbalance between the compressor and expansion valve as the valve is closing to achieve the superheat set point temperature. Comparisons between the pressure predictions and measurements indicate that the model can generally capture the refrigerant dynamics under defrosting operations and during the rapid state evolution of reverse flow.

Figure 6 shows the refrigerant mass flow rate prediction in the cycle liquid-line between the indoor coil and expansion valve. It is important to note that the refrigerant flow can be bi-directional in the liquid-line. Following the sign convention that inflow quantities are positive and outflow quantities are negative, a positive mass flow rate at the inlet of a component indicates the nominal flow direction (e.g., heating mode), while a negative flow rate indicates reverse flow (e.g., defrosting mode). The sign convention applies to both mass flow and heat flow in the following context. When the system initiates a defrost cycle at 158 min, a spike of the liquid-line flow rate occurs as the expansion valve is fully opened. The reversing valve is then engaged to trigger the flow reversal. The mass flow rate steadily increases during the defrost cycle since expansion valves are kept fully open as the reversed refrigerant flow develops, until the flow is reversed at the end of defrost cycle. Note that the output signal of the mass flow meter saturates to zero when the flow direction is opposite to the configured direction in the test. That means, the flow rate measurement during defrost cycle is unavailable.

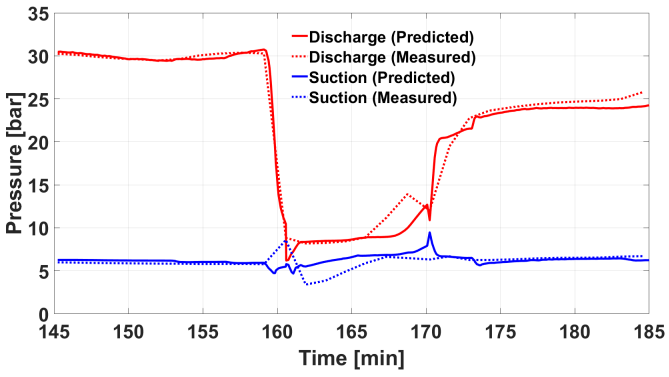

Figure 5: Validations of the refrigerant discharge and suction pressures.

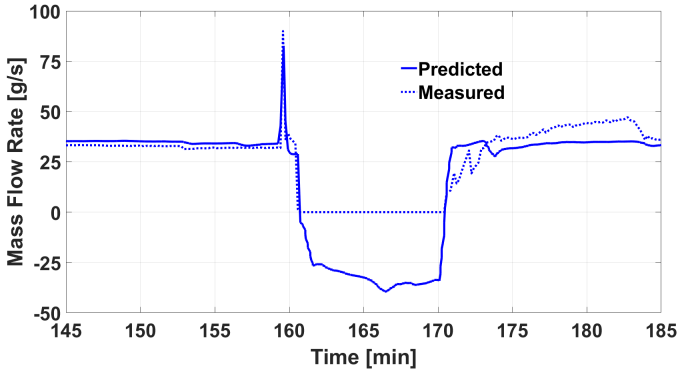

Figure 6: Liquid-line refrigerant mass flow rate.

Figure 7 reports validations of the compressor power and the indoor unit air-side capacity. The indoor unit fan is continuously running throughout the defrost cycle. The air-side capacity evolves corresponding to the refrigerant dynamics. In defrost mode, the indoor coil operates as an evaporator and the heat flow direction is reversed compared to heating mode. During this period, heat is removed from the indoor space, which can potentially result in thermal discomfort. The change of compressor power consumption follows regulation of the compressor speed, while also varying due to the refrigerant dynamics. The lower power consumption of defrost cycles can be attributed to the lower compressor speed and the smaller pressure ratio. The compressor power prediction agrees well with the measurement, though the model overestimates the air-side capacity during defrost cycle.

Figure 8 shows the simulated frost thickness and density trajectories associated with selected control volumes (CVs). Note that the CVs are indexed following the flow direction in heating mode, with CV1 representing the inlet connected to the expansion valve and CV30 representing the exit connected to the reversing valve. It can be seen that frost has larger thickness close to the liquid-line of the coil, where the refrigerant temperature is lower at the beginning of each frosting cycle. Correspondingly, the frost tends to be denser close to the vapor-line. During defrost cycles, the frost is considered to be completely melted when the thickness is smaller than 0.01 mm. Then the frost density is reset to 25 kg/m^3 to provide a reasonable initial condition for the next frosting cycle. After the defrost cycle, frost starts to accumulate as the system switches back to heating mode and the outdoor coil operates as an evaporator.

4. CONCLUSIONS

As a continuation of a companion paper (Ma et al., 2022), this paper reports simulation results of a complete air-source heat pump cycle model under reverse-cycle defrosting. A multi-stage frost melting model with a robust switching scheme is developed and integrated into a heat exchanger model that can switch between frost formation and melting

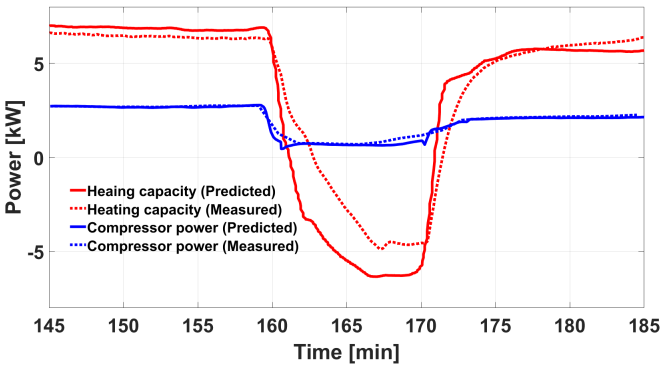

Figure 7: Validations of the compressor power and indoor unit air-side capacity.

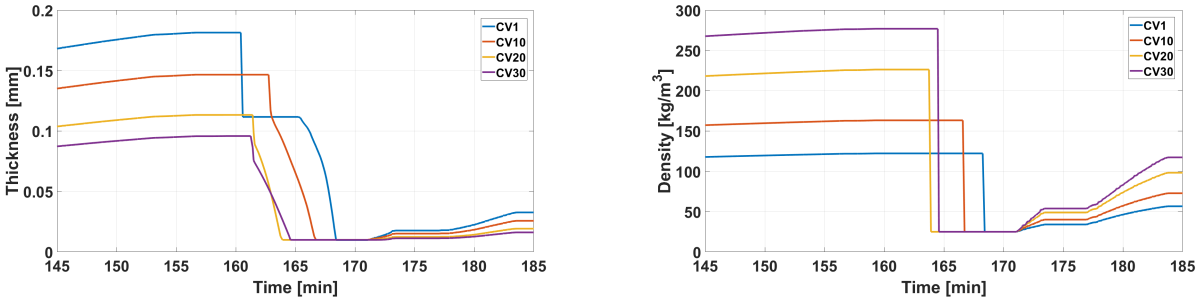

(a) (b)

Figure 8: Simulated frost properties of control volumes 1, 10, 20, 30: (a) frost thickness, (b) frost density.

dynamics. The heat pump cycle model is simulated to capture the defrost cycle dynamics as well as transitions between heating and defrosting cycles triggering reverse flow. Comparisons between the model predictions and measurements yield that the model can generally capture the complicated dynamics associated with reversed heat pump cycles and non-uniform frost deposition. The developed model is able to capture the cycling operations of heating and defrosting, without a need for reinitializing the system when the operating mode switches, which is attractive for development and evaluation of improved control and fault detection designs for heat pump units.

NOMENCLATURE

$\dot{m}$	Mass flow rate	[kg/s]
δ	Thickness	[m]
μ	Membership function	[−]
ρ	Density	[kg/m^3]
c_p	Specific heat capacity	[J/(kg K)]
k	Thermal conductivity	[W/(m K)]
p	Pressure	[Pa]
T	Temperature	[K]

Subscript

a	Air
f	Frost
in	Inlet
out	Outlet
w	Metal wall

REFERENCES

Damasceno, G., Rooke, S., & Goldschmidt, V. (1991). Effects of reversing valves on heat pump performance. *International journal of refrigeration*, *14*(2), 93–97.

Dopazo, J. A., Fernandez-Seara, J., Uhía, F. J., & Diz, R. (2010). Modelling and experimental validation of the hot-gas defrost process of an air-cooled evaporator. *International journal of refrigeration*, *33*(4), 829–839.

Han, B., Xiong, T., Xu, S., Liu, G., & Yan, G. (2022). Parametric study of a room air conditioner during defrosting cycle based on a modified defrosting model. *Energy*, *238*, 121658.

Kim, D., Ma, J., Braun, J. E., & Groll, E. A. (2021). Fuzzy modeling approach for transient vapor compression and expansion cycle simulation. *International Journal of Refrigeration*, *121*, 114–125.

Ma, J., Kim, D., & Braun, J. E. (2022). Improving robustness of transient heat exchanger models with non-uniform frost formation. *19th International Refrigeration and Air Conditioning Conference at Purdue, July 10-14, 2022*.

Mohs, W. F. (2013). *Heat and mass transfer during the melting process of a porous frost layer on a vertical surface*. University of Minnesota.

Qiao, H., Aute, V., & Radermacher, R. (2015). Transient modeling of a flash tank vapor injection heat pump system–part i: Model development. *International journal of refrigeration*, *49*, 169–182.

Qiao, H., Aute, V., & Radermacher, R. (2018). Modeling of transient characteristics of an air source heat pump with vapor injection during reverse-cycle defrosting. *International journal of Refrigeration*, *88*, 24–34.

Qu, M., Pan, D., Xia, L., Deng, S., & Jiang, Y. (2012). A study of the reverse cycle defrosting performance on a multi-circuit outdoor coil unit in an air source heat pump–part ii: Modeling analysis. *Applied Energy*, *91*(1), 274–280.

Steiner, A., & Rieberer, R. (2013). Parametric analysis of the defrosting process of a reversible heat pump system for electric vehicles. *Applied thermal engineering*, *61*(2), 393–400.

Zak, S. H. (2003). *Systems and control* (Vol. 198). Oxford University Press New York.

ACKNOWLEDGMENT

This work was supported by the Center for High Performance Buildings (CHPB) at Purdue University under the project number CHPB-49-2021.